Atmospheric
Chemistry
and Physics

Emission characteristics of refractory black carbon aerosols from fresh biomass burning: a perspective from laboratory experiments

Xiaole Pan[1], **Yugo Kanaya**[2], **Fumikazu Taketani**[2], **Takuma Miyakawa**[2], **Satoshi Inomata**[3], **Yuichi Komazaki**[2],
Hiroshi Tanimoto[3], **Zhe Wang**[1,4], **Itsushi Uno**[4], and **Zifa Wang**[1]

[1]State Key Laboratory of Atmospheric Boundary Layer Physics and Atmospheric Chemistry,
Institute of Atmospheric Physics, Chinese Academy of Sciences, Beijing, 100029, China
[2]Japan Agency for Marine-Earth Science and Technology, Yokohama, 236-0001, Japan
[3]National Institute for Environmental Studies, Tsukuba, 305-8506, Japan
[4]Research Institute for Applied Mechanics, Kyushu University, Kasuga, 816-8580, Japan

Correspondence to: Xiaole Pan (panxiaole@mail.iap.ac.cn)

Abstract. The emission characteristics of refractory black carbon (rBC) from biomass burning are essential information for numerical simulations of regional pollution and climate effects. We conducted combustion experiments in the laboratory to investigate the emission ratio and mixing state of rBC from the burning of wheat straw and rapeseed plants, which are the main crops cultivated in the Yangtze River Delta region of China. A single particle soot photometer (SP2) was used to measure rBC-containing particles at high temporal resolution and with high accuracy. The combustion state of each burning case was indicated by the modified combustion efficiency (MCE), which is calculated using the integrated enhancement of carbon dioxide and carbon monoxide concentrations relative to their background values. The mass size distribution of the rBC particles showed a lognormal shape with a mode mass equivalent diameter (MED) of 189 nm (ranging from 152 to 215 nm), assuming an rBC density of $1.8 \, \mathrm{g \, cm^{-3}}$. rBC particles less than 80 nm in size (the lower detection limit of the SP2) accounted for $\sim 5\%$ of the total rBC mass, on average. The emission ratios, which are expressed as $\Delta \mathrm{rBC} / \Delta \mathrm{CO}$ (Δ indicates the difference between the observed and background values), displayed a significant positive correlation with the MCE values and varied between 1.8 and $34 \, \mathrm{ng \, m^{-3} \, ppbv^{-1}}$. Multi-peak fitting analysis of the delay time (Δt, or the time of occurrence of the scattering peak minus that of the incandescence peak) distribution showed that rBC-containing particles with rBC MED $= 200 \pm 10$ nm displayed two peaks at $\Delta t = 1.7 \, \mu s$ and $\Delta t = 3.2 \, \mu s$, which could be attributed to the contributions from both flaming and smoldering combustion in each burning case. Both the Δt values and the shell/core ratios of the rBC-containing particles clearly increased as the MCE decreased from 0.98 (smoldering-dominant combustion) to 0.86 (flaming-dominant combustion), implying the great importance of the rapid condensation of semi-volatile organics. This laboratory study found that the mixing state of rBC particles from biomass burning strongly depends on its combustion processes, and overall MCE should be taken carefully into consideration while the climate effect of rBC particles from open biomass burning is simulated.

1 Introduction

Black carbon aerosols in the atmosphere play a vital role in climate change by absorbing solar radiation and altering the formation, lifespan and albedo of clouds (Novakov et al., 2005; Ramanathan and Carmichael, 2008; Bond et al., 2013). It was operationally defined according to its light absorption capacity, chemical reactivity and/or thermal stability (Lack et al., 2014). One definition is refractory black carbon (rBC), which corresponds to the carbon mass derived from laser-induced incandescence (LII) emission at a boiling point at 4000 K. Open biomass burning (which normally refers to burning of living or dead vegetation such as agriculture residue, grass, forest, leaves, and shrub due to anthropogenic

activities and natural causes, abbreviated as OBB) is one of the important sources of rBC, and it contributes ~42 % of atmospheric loadings in the global emissions budget (Bond et al., 2004). In addition to rBC, OBB also simultaneously emits substantial amounts of semi-volatile organics that undergo extremely complicated mixing processes with rBC during transport. Jacobson (2001) pointed out that the light absorption by internally coated rBC by inorganic/organic matter could increase, due to the "lensing effect", in which a non-absorbing coating directs more light to the cores of rBC particles. However, the debate on the absorption enhancement capacity of rBC-containing particles is still ongoing, because discrepancies exist between observations and theoretical predictions based on Mie scattering models (Shiraiwa et al., 2010; Cappa et al., 2012) and among observation results from different locations and using different sources (Healy et al., 2015; S. Liu et al., 2015; Massoli et al., 2015; Ueda et al., 2016). The widely accepted explanations are as follows. First, the morphologies of rBC particles differ among different sources, and the process of particle aging in the atmosphere changes the physical structure of the particles. For instance, several studies have found that rBC particles with a fractal structure tend to collapse to a more closely packed shape when they are thickly coated (Adachi et al., 2010; Chen et al., 2010; He et al., 2015). Modeling study indicated that hygroscopic growth of rBC-containing particles also results in more compact rBC cores (Fan et al., 2016). Second, the rBC particles sometimes were also reported to be attached on the surface of non-rBC matter (Moteki et al., 2014). Either of these circumstances renders the core–shell model invalid or introduces biases into the results. Sedlacek et al. (2012) reported that a large fraction (60 %) of rBC-containing particles with non-core–shell structures exist in biomass burning plumes. Methodologies have also been developed to distinguish particles with attached rBC (bare rBC on the surfaces of non-rBC particles) from rBC-containing particles with the core–shell structure (Moteki et al., 2014). In addition, OBB is an important source of brown carbon (BrC), which has distinct light absorbing features with different wavelength dependence, and their coexistence of rBC and BrC also influences the overall absorption enhancement of rBC-containing particles (Lack et al., 2012; Saleh et al., 2014; D. Liu et al., 2015; S. Liu et al., 2015; Saleh et al., 2015).

Biomass normally consists of cellulose/hemicellulose, organics and water. The emissions of rBC from OBB are determined by the composition (carbon content) of the biofuel and the evolution of combustion (Yokelson et al., 1997; Andreae and Merlet, 2001). Briefly, the combustion process of biomass begins with the pyrolysis of biofuel molecules and the evaporation of flammable mixtures (i.e., volatile compounds) and water, which is followed by flaming combustion that converts most carbon substances to carbon dioxide (CO$_2$). rBC particles are also produced in large quantities at this stage due to the oxygen-limited conditions and

high temperatures. The last stage is smoldering combustion, which predominantly emits carbon monoxide (CO) and organics (Andreae and Merlet, 2001). It was reported that "tar balls" that mostly consisted of BrC and secondary organic aerosols with low volatility were also emitted during smoldering combustion (Pósfai et al., 2004). Detailed descriptions of the physical properties of biomass burning particles have been provided in the literature (Reid et al., 2005; Akagi et al., 2011). The modified combustion efficiency (MCE), which is defined as $\Delta CO_2 / (\Delta CO_2 + \Delta CO)$ (Δ is the difference in measured concentrations between the OBB plume and the corresponding background value), has been used to indicate the relative amounts of flaming and smoldering combustion during a fire for characterizing the emission of rBC and organic matter. An MCE value > 0.95 is normally regarded as flaming-dominant combustion, whereas MCE < 0.9 represents smoldering-dominant combustion (Kondo et al., 2011; Pan et al., 2012, 2013; May et al., 2014).

The rBC emission ratio ($\Delta rBC / \Delta CO$), which is defined as the enhancement of mass concentration rBC (in unit ng m^{-3}) with respect to its background versus that of CO (in unit ppbv, parts per billion volume), is an applicable indicator for constraining the rBC emission inventory for models (Pan et al., 2011). The variability in $\Delta rBC / \Delta CO$ among observational studies mostly results from differences in measurement techniques, fuel type, and burning conditions. For example, observations made onboard the NOAA WP-3D aircraft yielded $\Delta rBC / \Delta CO$ values of 9 ± 2 ng m^{-3} ppbv^{-1} (Spackman et al., 2008) and 17.4 ng m^{-3} ppbv^{-1} (Schwarz et al., 2008) for brush fire plumes during the TexAQS field campaign. Airborne observations on the NASA DC-8 aircraft indicated that the $\Delta rBC / \Delta CO$ values were 8.5 ± 5.4 ng m^{-3} ppbv^{-1} for plume of boreal forest and agriculture fires in Asia, and 2.3 ± 2.2 ng m^{-3} ppbv^{-1} for wildfire plume in North America (Kondo et al., 2011). Observations using a multi-angle absorption photometer (MAAP, which employs the filter-based light absorption technique; here we consider BC instead of rBC) at mountain sites (30.16° N, 118.26° E; 1840 m a.s.l.) in South China yielded high $\Delta BC / \Delta CO$ values (10–14 ng m^{-3} ppbv^{-1}) when the site was subjected to burning of crop residues (Pan et al., 2011). The large variability also resulted from a difference in sampling altitude. For instance, airborne-based measurements tend to capture flaming-dominant plumes because they are more easily injected to high altitudes than smoldering-dominant plumes (Kondo et al., 2011). In fact, rBC emissions are heavily dependent on the combustion state of biomass. Field measurements using a semi-continuous ECOC analyzer (thermo-optical transmittance technique, IMPROVE protocol) during OBB episodes in East China yielded $\Delta EC / \Delta CO$ values of 17.4 ± 5.2 ng m^{-3} ppbv^{-1} for flaming-dominant cases and 11.8 ± 2.3 ng m^{-3} ppbv^{-1} for smoldering-dominant cases (Pan et al., 2012). Biomass burning experiments in the laboratory on 15 individual plant species sampled in the

United States indicated that $\Delta rBC / \Delta CO$ increased by up to $40\,ng\,m^{-3}\,ppbv^{-1}$ as MCE increased to 0.95, and this result was largely insensitive to the biomass type used (May et al., 2014). Note that $\Delta rBC / \Delta CO$ values decreased significantly with aging of OBB plumes, owing mostly to the below-cloud and in-cloud scavenging processes as a result of large fractions of water-soluble organic species (Mazzoleni et al., 2007; Gilardoni et al., 2016). Observations made in both East Asia and North America indicate a strong dependence of $\Delta rBC / \Delta CO$ on accumulated precipitation along backward trajectories (Kondo et al., 2011), implying that the rBC-containing particles became hydrophilic and were removed by wet deposition during transport. This result is consistent with observations of OBB plumes at the top of Mt. Tai (36.26° N, 117.11° E; 1534 m a.s.l.) in North China, which indicated that $\Delta BC / \Delta CO$ values for OBB plumes decreased substantially due to cloud scavenging processes (Pan et al., 2013).

The Yangtze River Delta region (YRDR) is one of the most important agricultural regions in China, and it accounts for 29 % of total grain production. Wheat and rapeseed plants are two major crops. After harvest, some of the crop straws are burned in the open air at fields, resulting in severe air pollution on the regional scale. Although field measurements of variations in the concentrations of rBC and CO and their ratios in OBB plumes have been reported, their physical characteristics may change significantly due to the rapid aging/mixing processes of semi-volatile organic vapors. Therefore, laboratory studies are very important to obtain insight into the initial emission features of rBC particles in China. In the present study, we conducted laboratory burning experiments using two crop residues (wheat straws and rapeseed plants) obtained from the YRDR. The mass concentration and size distribution of rBC particles in the OBB plume were measured using a single particle soot photometer (SP2). The physical properties of nascent rBC-containing particles, the evolution of the size distribution, the mixing state of the rBC particles, and their dependence on the combustion state were investigated. The information presented in this paper is helpful for constraining/reducing uncertainties in OBB emission inventories and the estimates of their climatic effects by models.

2 Experiments

2.1 Description of the burning experiments

We conducted burning experiments in the laboratory using samples of wheat straw and rapeseed plants that were collected in an agricultural area of East China during a field campaign in 2010 (Pan et al., 2012). All of the biomass was stored in sealed plastic bags to preserve its original state. During experiments, the biomass sample was placed on an aluminum foil net rack in a heat-resistant combustion

box with an approximate volume of 144 L, and it was ignited by a butane-fuel lighter from the bottom. Afterwards, the biomass burned until it went out completely. In general, a total of 24 samples (the mass of each sample was $\sim 20\,g$) were tested. The OBB smoke was removed from the room by a venting fan through a flexible rubber hose at a flow rate of $120\,m^3\,h^{-1}$. The wheat straw samples were classified into two groups. Twenty samples were burned in the chamber without artificial treatments, and four of the samples were placed in humid conditions (RH > 99 %) for 30 min to absorb moisture for comparison. Detailed information on the setup of the OBB experiments is provided in the literature (Inomata et al., 2015). As mentioned, MCE is a useful metric for describing the combustion phase of biomass burning, and the calculation of MCE requires simultaneous measurements of CO and CO_2 concentration. Here, the mixing ratio of CO_2 was measured using a Li-7000 CO_2 analyzer (Li-COR Inc.; detection range 0–3000 ppmv, RMS noise 35 ppbv, integration time 0.5 s) through a separate 1/8 inch, $\sim 1.5\,m$ long Teflon tube. The mixing ratio of CO was concurrently measured with an ultrafast CO analyzer (model AL5002, Aero-Laser GmbH; detection range 0–100 ppmv, detection limit 1.5 ppbv, integration time 1 s). Comparison with a non-dispersive infrared CO gas analyzer (Thermo 48C; precision 10.0 ppbv, RMS noise 5.0 ppbv, average time 1 min) indicated that the measurement uncertainty was within 5 %.

To avoid instrument overloading due to the extremely high concentrations of particles and trace gases, the inlets of the sampling lines were situated $\sim 40\,cm$ away from the combustion smoke. The sampling flows were subsequently diluted in a dilution system by mixing dry zero air produced by a zero gas generator (Thermo Inc., model 111). The flow rate of injected zero air was precisely controlled with a mass flow controller (Kofloc Inc., model 3660; accuracy $\pm 1.0\,\%$ at 25 °C). The uncertainty of the dilution system was evaluated using known-size dry polystyrene sphere latex particles (PSL, size standard particles, JSR Corporation, Japan). The PSL aerosols were produced by a nebulizer at a flow rate of $3.5\,L\,min^{-1}$, passed through a diffusion dryer (model 3062, TSI Inc., USA) and then size-selected using a differential mobility analyzer (DMA, model 3081, TSI Inc., USA). The number concentration of PSL particles was measured using a laser aerosol spectrometer (LAS-X II, PMS(GB) Ltd., UK; uncertainty 5 %, flow rate 50 ccm) with and without dilution. The errors of the dilution system were found to be 6, 2, 2, 4, and 5 % for particles with mobility diameters of 120, 200, 300, 500, and 1000 nm, respectively, at a dilution ratio of ~ 50. During the burning experiment, a 50 cm long, 1/4 inch flexible conductive silicone tube (TSI Inc., USA) and stainless steel Swagelok fittings were used for the aerosol tubing (dilution factor: 46), and a polytetrafluoroethylene (PTFE) tube and fittings were used for the measurement of gases (dilution factor: 22). Abbreviations and symbols used in this paper are shown in Table 1.

Table 1. Abbreviations and symbols used in this paper.

Symbol/ abbreviation	Full name/explanation
rBC	Refractory black carbon, as derived using the LII method at a temperature of ~ 4000 K.
Δt	The delay in the time of occurrence of the incandescence peak *after* that of the peak of the scattering signal
APM	Aerosol particle mass analyzer (Kanomax Inc.)
S/C ratio	Shell/core ratio
CO	Carbon monoxide
CO_2	Carbon dioxide
C_S	Scattering cross section
DMA	Differential mobility analyzer (TSI Inc.)
FS	Fullerene soot (C60)
LEO fitting	Leading-edge-only fitting method proposed by Gao et al. (2007)
LSP	Light scattering particle
MCE	Modified combustion efficiency
MED	Mass equivalent diameter
MMD	Mass mode diameter
non-rBC	Non-refractory black carbon matter that evaporates as rBC absorbs energy
OBB	Open biomass burning
SP2	Single particle soot photometer (DMT Technologies)

2.2 Instruments

2.2.1 Single particle soot photometer

A single-particle soot photometer (SP2, Droplet Measurement Technologies Inc.) was used to examine the evolution of the number concentration and mixing state of the OBB particles. The SP2 employs a continuous intracavity Nd:YAG laser beam (1064 nm, TEM00 mode, Gaussian) to produce a strong laser power field and detects the laser-induced incandescence signal emitted from individual rBC particles when they are heated to their boiling point (~ 4300 K) (Gao et al., 2007). The peak value of the incandescent signal was converted to the rBC mass based on a calibration curve determined using fullerene soot (FS) particles (stock 40 971, lot: L20W054, Alfa Aesar, USA). The calibration procedure used in quantifying rBC masses was the same as that used in previous studies (Moteki and Kondo, 2010; Miyakawa et al., 2016). The effective density function of FS was determined on the basis of a DMA–aerosol particle mass (DMA–APM) system in Yutaka Kondo's laboratory at the University of Tokyo and was consistent with previous results (Moteki and Kondo, 2007; Gysel et al., 2011) (Fig. S1 in the Supplement). In our study, the mass of the individual FS particles ranged from 0.35 to 89.5 fg, which corresponds to 80–700 nm in mass equivalent diameter (MED), assuming an rBC density of 1.8 g cm^{-3} and ideally spherical particles.

Due to variations in morphology and composition under ambient conditions, the incandescent signal may not always be linearly proportional to the mass of rBC particles. The uncertainty of the derived rBC mass on the basis of the incandescent signal was estimated to be ~ 30 %, and the uncertainty of the derived MED values was estimated to be ~ 10 %. The mass size distribution of the rBC in the OBB plume typically peaked at 180–200 nm (< 10 fg). Extrapolation using a lognormal function fit to the observed size distribution suggested that the missing rBC particles with MED < 80 nm and MED > 500 nm only cause minor mass underestimation (~ 5 %). The size-dependent detection efficiency of SP2 for FS particles was also evaluated on the basis of a DMA-SP2-CPC (model 3010, TSI Inc., USA) system, and we found that the SP2 detection efficiency was in the range of 0.94–0.98 for particles with MED values larger than 80 nm (shown in Fig. S2).

The scattering signal of the SP2 was calibrated using PSL particles with known sizes (170, 200, 254, 300, 500 and 1000 nm). It is worth noting that only PSL particles with sizes larger than 166 nm can be detected adequately, implying that the ambient measurement of the SP2 will underestimate the total number concentration of light-scattering particles because the particles that are smaller than this size threshold are not counted. A two-elemental avalanche photodetector was employed in the SP2 to determine the actual position of the particle in the laser beam, which allows for delay time and coating thickness analysis of rBC particles with a core–shell structure (Gao et al., 2007). Detailed information on the SP2 is provided in the literature (Schwarz et al., 2008, 2010; Moteki et al., 2014).

2.2.2 Determination of the coating thicknesses of rBC-containing particles

As mentioned above, when the rBC-containing particles pass through the laser beam, the rBC component needs a short period of time to absorb energy to gradually evaporate the coating materials. This means that the time when the rBC reached its boiling point was later than the time of occurrence of the peak of scattering. For the rBC-containing particles with core–shell structures, the coating thickness can be semi-qualitatively represented by the delay time of the LII peak (Δt), which is defined as the elapsed time between the occurrence of the peak of the scattering signal and the peak of the incandescence signal; a positive value of this quantity indicates that the peak of the incandescence signal occurs after the peak of the scattering signal. In principle, the larger the Δt value is, the more likely the rBC core is to be thickly coated. Such phenomena have been frequently reported in a number of studies (Moteki et al., 2007; Subramanian et al., 2010). In our experiment, a histogram analysis of the Δt value demonstrated that there was a small Δt^* peak at 0.8 ± 0.5 (2σ) µs for the uncoated FS particle with MED < 400 nm. Apparently, this Δt^* peak did not result

from the coating effect, but the intrinsic error of the photodetector of the SP2. We regarded the particles with Δt values larger than 1.3 (mean $+ 2\sigma$) μs as being coated. A detailed classification of thinly coated and thickly coated particles is discussed in Sect. 3.4. In practice, estimation of the coating thickness of rBC cores in terms of Δt values is sometimes problematic because, first, the Δt values showed a discontinuous increase with an increase in coating thickness, depending on both the rBC core and the coating material. A laboratory study of graphite particles coated with organic liquids indicated that the Δt value jumped from less than 1 to 3 μs after the coating thickness of particles exceeded a threshold value (Moteki and Kondo, 2007). Such variations provide only a measure of the minimum detectable coating thickness, and they do not permit precise estimation. Second, the Δt value can be negative in cases where the peak of the incandescence signal occurs *before* the peak of the scattering signal (Sedlacek et al., 2012). Negative Δt values have been reported not only in biomass burning plumes (Sedlacek et al., 2015) but also in laboratory experiments (Moteki and Kondo, 2007). An accepted explanation is that the rBC component is located at or near the surface of non-refractory matter (such particles are said to belong to the non-core–shell type or the attached type). When such particles passed through the laser beam, the rBC did not absorb a sufficient amount of energy to evaporate the non-rBC substances, and the occurrence of fragmentation allowed some of the remaining non-rBC substances to pass though the laser, producing a scattering signal after the incandescence signal was induced. Moteki et al. (2014) suggested the use of the time-dependent variation of the scattering cross section (C_s) to differentiate the coated rBC particles from the attached type and proposed a measurable parameter, a logarithm of the ratio of C_s before evaporation (C_{s-be}) to C_s at the onset of incandescence (C_{s-oi}), $\log(C_{s-be}/C_{s-oi})$, to quantify the contributions from the different types.

Following the same principle, we calculated the coating thicknesses of rBC-containing particles with the core–shell structure on the basis of the leading-edge-only (LEO) fitting method (Gao et al., 2007). The physical interpretation of this method has been described in the literature (Gao et al., 2007; Laborde et al., 2012). In the LEO fitting approach, the laser intensity profile of the SP2 was predetermined from an analysis of the PSL particles, and the "leading edge" data are selected according to the criterion of $t < -2.5\sigma$. Here, σ denotes the standard deviation of the Gaussian function of the laser intensity profile. Using a strict threshold (e.g., $t < -3\sigma$) can reduce the risk of the onset of evaporation of the coating; however, it significantly increases the possibility of incorrect Gaussian fitting. The optical diameter of the undisturbed rBC-containing particles was estimated using Mie scattering theory and the LEO-fitted scattering peak height, presuming a refractive index of $m = 1.5 - 0i$ for the coating materials. To test the validity of the LEO fitting method, laboratory experiments were performed using FS particles (Alfa Aesar 40971, lot: L20W054) coated with oleic acid (molec-

ular weight 282.46, boiling point 360 °C). The instruments used in this procedure are the same as those described in the literature (Moteki and Kondo, 2007). FS particles with mobility diameters of 100, 150, and 200 nm were selected using the DMA and then coated with oleic acid using a heated oleic oil bath. The coated particles with shell mobility diameters of 180, 200, 250, 300, and 350 nm were selected by a second DMA and then measured using the SP2. We excluded the doubly charged particles from the data analysis because both the core and shell sizes of these particles were apparently larger than those of the singly charged ones. The shell diameters of the coated particles were well determined using the LEO fitting method. Linear regression analysis of the calculated and measured shell diameters demonstrated a good positive correlation with a high correlation coefficient ($r^2 = 0.9$), as shown in Fig. S3. The coating thickness of rBC was calculated using $(D_p - D_c)/2$, where D_p and D_c are the shell and core diameters, respectively, of the rBC-containing particles. The shell / core (S/C) ratios were calculated using D_p/D_c. The total uncertainty of the S/C ratio values was calculated to be 14 %.

2.2.3 Non-methane volatile organic compounds (NMVOCs)

In the present study, the mixing ratios of the NMVOCs in the gas phase in the OBB smoke were measured simultaneously using a high-sensitivity proton-transfer-reaction mass spectrometer (PTR-QMS 500, IONICON Analytik GmbH) with a time resolution of 1.9 s. Four primary ions ($H_3^{18}O^+$, NO^+, O_2^+ and $H^+ \bullet (H_2O)_2$) were used, and more than 20 product ions (NMVOC $\bullet H^+$) were selectively monitored, according to predetermined multiple ion detection (MID) settings. The detection limit and dwell time of PTR-QMS for NMVOCs were generally less than 0.3 ppbv and 0.1 s, which are fully satisfactory for the measurement of OBB smoke. Detailed information on the configuration of the instrument is provided in the literature (Inomata et al., 2015).

2.3 Determination of combustion states and the rBC emission ratios

As mentioned, the excess mixing ratios of CO (ΔCO) and CO_2 (ΔCO_2) are normally used to estimate the modified combustion efficiency (MCE) of biomass, which was defined as $\Delta CO_2/(\Delta CO_2 + \Delta CO)$. In the present study, the mixing ratios of CO and CO_2 were measured at a time resolution of 1 s. Although the real-time variation in MCE was obtained, comparisons were difficult because the combustion states and durations varied significantly among the different cases. Here, a fire-integrated modified combustion efficiency
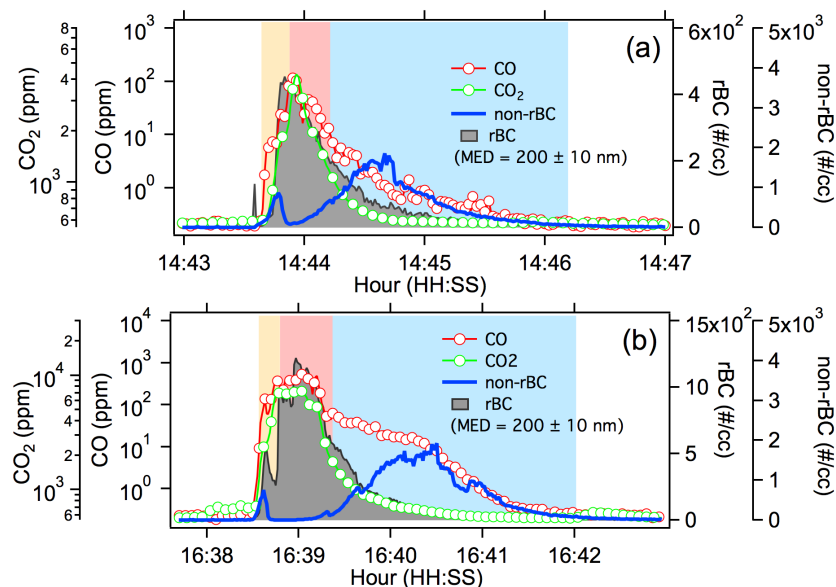
Figure 1. Temporal variations in the mixing ratios of CO and CO_2, and the number concentrations of rBC and non-rBC particles for the burning of wheat straw **(a)** and rapeseed plants **(b)**. The yellow (dry distillation step of the biomass), red (flaming-dominant combustion) and blue (smoldering-dominant combustion) shaded areas in the plot represent the different burning states.

was calculated on the basis of Eq. (1).

$$MCE = \frac{\sum \Delta CO_2}{\sum \Delta CO + \sum \Delta CO_2} \qquad (1)$$

$$= \frac{\sum \left([CO_2]_{plume} - [CO_2]_{baseline}\right)}{\sum \left([CO]_{plume}[CO]_{baseline}\right) + \sum \left([CO_2]_{plume} - [CO_2]_{baseline}\right)},$$

where $\sum$ represents the time-integrated total mixing ratios of ΔCO and ΔCO_2, and $[X]$ is the mixing ratio of species X, expressed as ppmv. Correspondingly, the emission characteristics of rBC were indicated by the rBC emission factor $\Delta rBC / \Delta CO$, which was calculated on the basis of Eq. (2).

$$\Delta rBC/\Delta CO = \frac{\sum \left([rBC]_{plume}[rBC]_{baseline}\right)}{\sum \left([CO]_{plume}[CO]_{baseline}\right)}, \qquad (2)$$

where [rBC] is the mass concentration of rBC in unit ng m^{-3}. The baseline of the mass concentration of rBC and the mixing ratios of CO and CO_2 were determined from the linear interpolation of the data before and after each combustion experiment.

3   Results and discussion

3.1   Evolution of the combustion process

Figure 1 shows two sample time series of the number concentrations of rBC and non-rBC particles and the mixing ratios of CO and CO_2 in the smoke for a wheat straw combustion case (Fig. 1a) and a rapeseed plant combustion case

(Fig. 1b). The evolution of the concentrations of particles and gases were similar, although the carbon content and combustion duration differed between the two biomass types. This result indicates that the combustion process was overwhelmingly important in determining the variations in emission characteristics. As described in the literature (Andreae and Merlet, 2001; Reid et al., 2005), smoldering combustion normally occurs after flaming-dominant combustion ceases, resulting in two isolated peaks for the mixing ratios of CO and CO_2. However, we did not observe such a clear boundary between these two stages in our burning experiments. This result occurred primarily because the combustion durations were short (less than 200 s), and both flaming and smoldering combustion might occur simultaneously in different parts of the biomass. The mixing ratios of CO displayed a broader tail than those of CO_2, implying that the relative importance of smoldering combustion increased at the end; this effect is particularly clear in Fig. 1b.

The temporal variations in the number concentration of rBC were highly correlated with those of CO_2. This phenomenon is in accordance with previous conclusions that the production of rBC particles is mostly related to flaming-dominant combustion processes (Pan et al., 2012). In the high-temperature and low-oxygen environment present in the inner part of flames, the evaporated unsaturated alkanes tend to pyrolyze to soot precursor particles (i.e., PAHs), which is followed by the aggregation and considerable growth of the rBC particles. The non-rBC particles appear to be mostly emitted under low-temperature burning conditions (Reid et al., 2005). Directly after the biomass was ignited, a small

peak (yellow shading in Fig. 1) in the number concentration was sometimes observed, which could be related to the emissions from combustion of butane fuel of lighters. As flaming temperature increased up to 800 K, rBC particles were produced in significant quantities, and these particles provided substantial numbers of condensation nuclei for semivolatile compounds. As a result, the number concentration of non-rBC particles decreased to almost zero (red shading in Fig. 1). When combustion shifted from the flaming-dominant to smoldering-dominant stage during the second half of the burning period (blue shading in Fig. 1), the number concentration of non-rBC particles increased again. This observation can be explained by the secondary condensation growth of pyrolyzed compounds that occurred because the temperature was not high enough to cause their complete oxidation. The number size distribution and volume size distribution of non-rBC particles during burning experiments are shown in Fig. S4. Overall, these observations confirmed the results of previous studies that indicate that particle formation in OBB is essentially a nuclei-limited condensation process, and rBC and CO_2 were mostly produced by flaming combustion, whereas organic matter and CO were emitted from the smoldering combustion (Reid et al., 2005).

Table 2 summarizes the information on the sample types, the mixing ratios of CO and CO_2, the mass concentration of rBC particles and MCE for all burning experiments. Although the combustion proceeded generally from flaming to smoldering phase, both flaming and smoldering combustion sometimes occurred at the same time at different positions of fuel. In addition, the durations of flaming or smoldering were different case by case. Here, the fire-integrated MCE value was used to represent the overall combustion condition for each combustion case. As shown, the averaged MCEs have no significant differences for the combustion of dry wheat straw (0.86–0.98), wet wheat straw (0.88–0.96), and dry rapeseed plants (0.91–0.96). The average mass concentration of rBC after 46 times dilution ranged from 0.25 to 19.8 $\mu g\,m^{-3}$, and the average mixing ratio of CO after 22 times dilution ranged from 95 to 5003 ppbv.

3.2 Variations in rBC size as a function of MCE

The masses of rBC particles as a function of mass equivalent diameter (MED) displayed a lognormal distribution for all burning cases. For better expression, each $dM/d\log Dp$ distribution was normalized so that its maximum value equalled 1 (Fig. 2a). We found that the mass mode diameter (MMD) for each combustion case clearly increased from 152 nm to 215 nm as the overall MCE value increased from 0.862 to 0.964. The correlation ($r^2 = 0.59$) was significant at the 95 % confidence interval (Fig. 2b). This result indicates that flaming combustion tends to produce larger rBC particles than smoldering combustion. It is consistent with previous studies, which reported that rBC particles formed considerably in intense flaming combustion due to less efficient transport
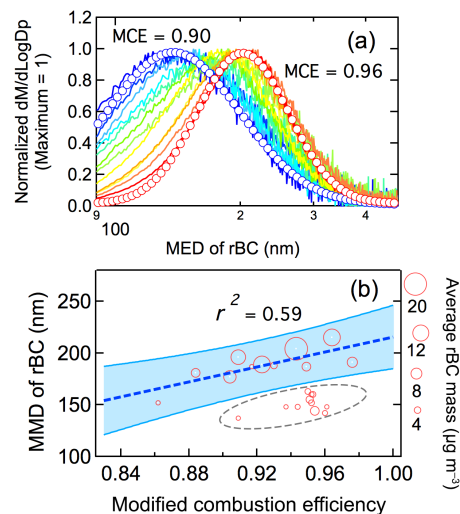

Figure 2. Normalized mass size distribution (maximum value = 1) of rBC particles for each burning experiment **(a)**. For better understanding, lognormal curve fittings are shown for a flaming-dominant combustion case (red circle) and a smoldering combustion-dominant case (blue circle). Variation of mode mass equivalent diameter (MMD) as a function of the modified combustion efficiency **(b)**. The size of the circle indicates the average rBC mass concentration for each burning case. Blue dashed line and blue shaded area are the linear fitting and confidence interval for fit coefficients. The data in the gray dashed circle are excluded in the linear fitting because of their low rBC mass concentrations.

of oxygen into the interior flame zone. As a result, growth in the size of rBC particles was rapid because the coagulation rate of particles is roughly proportional to the square of their number concentration (Lee and Chen, 1984). In this study, these consecutive processes were interrelated and could not be decoupled in the analysis. Nevertheless, this mechanism explained the outliers (contained within the dashed ellipse shown in Fig. 2b), in that the number concentration of rBC particles was not sufficient to support substantial growth. For smoldering combustion, the production of rBC precursors (i.e., PAHs) was less effective because of the low temperature.

As mentioned, the MMD of rBC particles in OBB plumes was determined by the combustion condition; however, its variations during the evolution of the OBB combustion process have not been fully investigated, because the separation of the combustion stage for in situ measurement was difficult. A recent study (Taylor et al., 2014) reported that the MMD of rBC particles was 152 nm. This value is apparently smaller than the frequently presented values (180–200 nm), and the authors attributed the differences to nucleation scavenging processes during transport. Published studies on OBB plumes are mostly based on airborne SP2 measurements. Andreae and Merlet (2001) noted that airborne measurements tend to be biased toward flaming combus-

Table 2. Description of sample types; overall combustion states; CO, CO_2, and rBC concentrations; MMD and geometric standard deviation (g_σ) of rBC; and emission ratios for the burning experiments. The ordering of these quantities is the same as in previous studies (Inomata et al., 2015).

No.	Sample[a] type	MCE [10th, 90th]	Duration Second	CO[b] ppbv	CO_2 ppmv	rBC[c] ng m^{-3}	rBC / CO ng m^{-3} ppbv^{-1}	rBC / CO_2 ng m^{-3} ppmv^{-1}	MMD[d] nm	g_σ
1	A	0.964 [0.941, 0.991]	164	1181	695	13 983	24.2	904.8	215	1.32
2	A	0.930 [0.909, 0.982]	122	311	91	2366	15.6	1171.5	188	1.46
3	A	0.952 [0.884, 0.973]	94	261	114	1446	11.3	570.4	152	1.44
4	A	0.949 [0.913, 0.999]	150	343	141	4812	28.7	1541.0	187	1.44
7	A	0.953 [0.830, 0.987]	123	256	114	1408	11.2	554.6	160	1.42
8	A	0.976 [0.960, 0.994]	184	380	340	6290	33.9	832.6	191	1.37
9	A	0.917 [0.900, 0.987]	121	189	46	168	1.8	165.3	187	1.47
10	A	0.944 [0.911, 0.979]	120	274	101	787	5.9	348.9	148	1.43
11	A	0.862 [0.828, 0.920]	125	464	64	470	2.1	331.8	152	1.44
12	A	0.937 [0.853, 0.988]	151	230	75	429	3.8	256.5	148	1.42
13	A	0.950 [0.896, 0.976]	143	282	118	1790	13.0	682.8	163	1.46
14	A	0.952 [0.837, 0.964]	158	290	126	1295	9.1	461.1	160	1.50
15	B	0.909 [0.881, 0.999]	220	4757	1045	11 255	4.8	484.5	196	1.33
16	B	0.904 [0.857, 0.999]	207	1339	277	8658	13.2	–	177	1.36
17	B	0.961 [0.840, 0.988]	97	75	41	250	6.8	276.2	148	1.45
18	B	0.884 [0.730, 0.999]	230	1373	230	5350	8.0	1045.7	181	1.41
19	C	0.943 [0.902, 0.999]	244	2702	983	19 802	15.0	906.0	204	1.29
20	C	0.923 [0.891, 0.999]	226	3512	926	13 402	7.8	651.2	189	1.33
21	C	0.909 [0.839, 0.947]	258	286	63	209	1.5	149.6	137	1.39
22	C	0.951 [0.895, 0.976]	188	956	408	3052	6.5	336.4	155	1.41
23	C	0.960 [0.874, 0.985]	172	457	241	1259	5.6	234.9	142	1.44
24	C	0.954 [0.944, 0.994]	191	846	386	4609	11.1	537.4	144	1.47

[a] Sample type: wheat straw/dry (A), wheat straw/wet (B), rapeseed plant/dry(C); [b] the mixing ratio of CO was diluted by 22 times; [c] the mass concentration of rBC was diluted by 46 times; [d] mode diameter in mass size distribution of rBC, abbreviated as MMD.

tion because the plumes formed during the flaming stage were more likely to be injected to higher altitudes than those formed during the smoldering stage (Kondo et al., 2011). Another explanation involved rapid coagulation processes, in which small rBC monomers might easily form agglomerates or clusters driven by organic coatings when the temperature of the plume decreased. This process likely occurs so quickly (on the timescale of seconds) that ambient measurements (OBB plume age > 1 h) cannot detect this process.

3.3 Emission ratio of rBC particles

Figure 3 shows the dependence of the ΔrBC / ΔCO ratio on the MCE for all combustion cases. For comparison, the results from previous OBB experiments in the laboratory, as well as from field measurements and emission inventories, are also plotted in the same figure. As shown, the ΔrBC / ΔCO ratio increased from 1.5 ng m^{-3} ppbv^{-1} to 34 ng m^{-3} ppb^{-1} as the MCE increased from 0.91 to 0.98. The results of fitting a power function were similar to those from previous studies (McMeeking et al., 2009; May et al., 2014), even though different types of biomass were combusted. This result indicates that the MCE value is a key parameter for determining the rBC emission intensity from

OBB, irrespective of the difference in the types of biomass used. In the present study, we tested two biomass conditions (dry and wet) for wheat straw. For combustion cases involving wet wheat straw, we found that the values of the ΔrBC / ΔCO ratio were always less than 7.1 ng m^{-3} ppbv^{-1} as the MCE value increased up to 0.96, and these values are much smaller than that (25.3 ng m^{-3} ppbv^{-1}) corresponding to dry wheat straw. This result implies that the wet biomass was unfavorable for the production of rBC particles. This phenomenon is consistent with the experimental results described by Chen et al. (2010), who reported an evident decrease in the emission factor of elemental carbon and a moderate increase in the emission factor of CO for burning of moist wildland biomass.

In this study, the average ΔrBC / ΔCO ratio was 13.9 ± 10.1 ng m^{-3} ppbv^{-1} for the burning cases with a fire-integrated MCE > 0.95. This value was probably a low estimation since both flaming and smoldering combustions were included in the calculation. However, by selecting the cases with both the 10th and 90th percentiles' MCE value > 0.90, we found that the average ΔrBC / ΔCO ratio was 23.1 ± 11.4 ng m^{-3} ppbv^{-1}, higher than the value reported from airborne measurements (8.5 ± 5.4 ng m^{-3} ppbv^{-1}) for the outflowing aged OBB plumes observed in Asia dur-
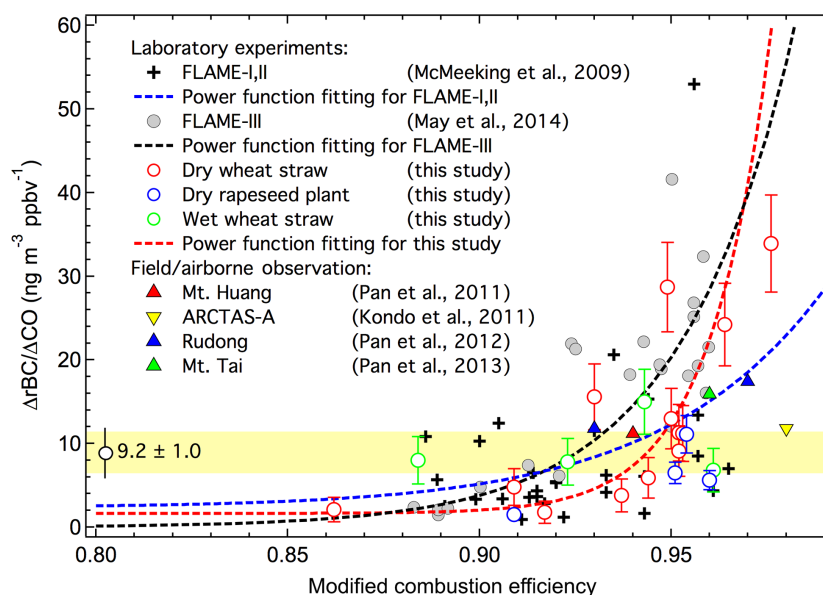
Figure 3. The variations in the emission ratios of rBC and ΔrBC / ΔCO, as a function of averaged MCE for all burning cases. Previous observations and the results of laboratory burning experiments are displayed in the plot.

ing ARCTAS-A (Kondo et al., 2011) and the value $(10 \pm 5 \, \text{ng m}^{-3} \, \text{ppbv}^{-1})$ for agricultural fires in Kazakhstan during ARCPAC (Warneke et al., 2009). In these studies, the OBB plumes were sampled after they had undergone a week of transport. In-cloud scavenging may take effect at these relatively low values, although precipitation had not occurred. The ΔrBC / ΔCO ratios derived from the FLAME-I and II experiments (McMeeking et al., 2009) are smaller $(8.3 \pm 9.7 \, \text{ng m}^{-3} \, \text{ppbv}^{-1}$ as converted from emission factors, expressed as g species kg^{-1} dry fuel), probably because the combustion was inclined to smoldering (average MCE = 0.92). In situ measurements of OBB plumes at the location where our samples for burning were collected (Pan et al., 2012) indicated that the ΔEC / ΔCO ratio from flaming-dominant burning was $17.4 \pm 5.2 \, \text{ng m}^{-3} \, \text{ppbv}^{-1}$. This result approximates those obtained in the laboratory. Measurements of OBB plumes in the North China Plain found that the ΔEC / ΔCO ratios from wheat straw burning ranged from 15 to 17 ng m^{-3} ppbv^{-1} (Pan et al., 2013). Kondo et al. (2011) reported ΔrBC / ΔCO ratios as low as $2.86 \pm 0.35 \, \text{ng m}^{-3} \, \text{ppbv}^{-1}$ (MCE = 0.96) for a fresh OBB plume in North America. These large discrepancies might result from significant rBC losses during transport. The yellow shading in Fig. 3 indicates the variability of ΔrBC / ΔCO ratios used in emission inventories. Comprehensive analyses including all kinds of OBB showed that the ΔrBC / ΔCO ratios were $8.6 \pm 1.2 \, \text{ng m}^{-3} \, \text{ppbv}^{-1}$ (as converted from emission factors, assuming a molar volume of 22.4 L at standard temperature and pressure conditions for CO) (Andreae and Merlet, 2001), $7.5 \pm 1.3 \, \text{ng m}^{-3} \, \text{ppbv}^{-1}$ (Akagi et al., 2011), and $9.0 \pm 1.6 \, \text{ng m}^{-3} \, \text{ppbv}^{-1}$ using the bottom–up method

(Yan et al., 2006). Synoptically speaking, a relatively high rBC emission ratio was suggested for estimating emission inventories of OBB because the majority of rBC emissions normally occur during the flaming combustion stage, despite the longer duration of the smoldering stage.

The emissions of rBC relative to ΔCO_2 were also calculated for each burning case (see Table 2). In general, the ΔrBC / ΔCO_2 ratios did not show a clear increase with increasing MCE values, and they varied from 149 to 1541 ng m^{-3} ppmv^{-1}, with a mean value of $592.5 \pm 364.1 \, \text{ng m}^{-3} \, \text{ppmv}^{-1}$. Schwarz et al. (2008) reported a high ΔrBC / ΔCO_2 ratio of $1770 \pm 400 \, \text{ng m}^{-3} \, \text{ppmv}^{-1}$, much higher than the values obtained in this study. Small values were also reported for OBB plumes observed in North America (100–357 ng m^{-3} ppmv^{-1}), Siberia (167 ng m^{-3} ppmv^{-1}) (Kondo et al., 2011), and China (245 ng m^{-3} ppmv^{-1}) (Pan et al., 2012). Despite the differences among these values, the ΔrBC / ΔCO_2 ratio remains a useful parameter in constraining the uncertainty of emissions of rBC from OBB to within an order of magnitude in models.

3.4 Delay time of incandescence

For the rBC-containing particles, the delay time (Δt) of the peak of the incandescent signal *after* that of the scattering signal is widely accepted as a proxy for the coating thickness of rBC particles. Particular caution should be employed when this concept is applied in data exploration. First, SP2 cannot detect particles with shell diameters less than 166 nm (the lower detection limit of SP2) owing to their weak scatter-

ing signal. A systematic bias always occurs when investigating the coating of rBC-containing particles with small rBC cores (i.e., MED less than 100 nm) because only very thickly coated rBC particles can be counted. To avoid this bias, we report only the rBC-containing particles with relatively large rBC cores (MED $= 200 \pm 10$ nm). Second, only the rBC-containing particles with positive Δt values were technically deemed as having a core–shell structure, to which the delay time-based method and LEO fitting method could be appropriately applied. In general, the scattering profile of rBC particles in the core–shell structure contained a main peak with a shoulder peak, which resulted from the coating material and the rBC core, respectively. If there was only one predominant scattering peak with a quasi-Gaussian shape, it suggested that the evaporation of non-rBC coatings was insignificant, and the rBC-containing particle likely belonged to the attached type, as demonstrated in the literature (Moteki et al., 2014). In this study, the shell diameters of rBC-containing particles with the core–shell structure were estimated using the LEO fitting method (described in Sect. 2.2.2). We found that the shell diameters of rBC-containing particles with rBC cores having MED $= 200$ nm ranged from 210 to 400 nm, with a 5th percentile value of 218 nm and a 95th percentile value of 330 nm. The corresponding shell/core (S/C) ratios were between 1.09 and 1.7.

The dependencies of Δt on the derived S/C ratios of all of the coated rBC particles for all of the burning experiments are shown in Fig. 4. The color in the plot represents the total number count of particles in each bin. In general, Δt increases as the S/C ratio increases, reflecting the fact that the rBC particles must spend a longer period of time absorbing energy to evaporate thicker coatings. Histogram analysis showed that both the S/C ratio and Δt displayed neither simple Gaussian nor lognormal distributions. Instead, a multiple-peak Gaussian provided a good fit to their number distributions (Fig. 4). For the distribution of the S/C ratio, there were two modes. One mode (no. 1) occurs at an S/C ratio $= 1.18$, and another mode (no. 2) occurs at an S/C ratio $= 1.34$, indicating that the rBC particles had different levels of coatings. The differences in coating thickness were most likely related to the combustion state of biomass burning. As mentioned, although flaming combustion emitted a substantial amount of semi-volatile organic carbons, the production of rBC particles was also significant at high temperatures. The competing condensing processes under nuclei-rich conditions resulted in relatively thin coatings on the rBC particles, instead of direct formation of particulate organic matter. Previous studies (Kudo et al., 2014; Inomata et al., 2015) also found that the emission factor of NMVOCs during the flaming stage was lower by an order of magnitude than that during the smoldering stage. It also supported our conclusion that the thinly coated rBC particles associated with mode no. 1 and mode no. 2 were primarily related to the flaming combustion and smoldering combustion stages, respectively. In the present study, the integrated area
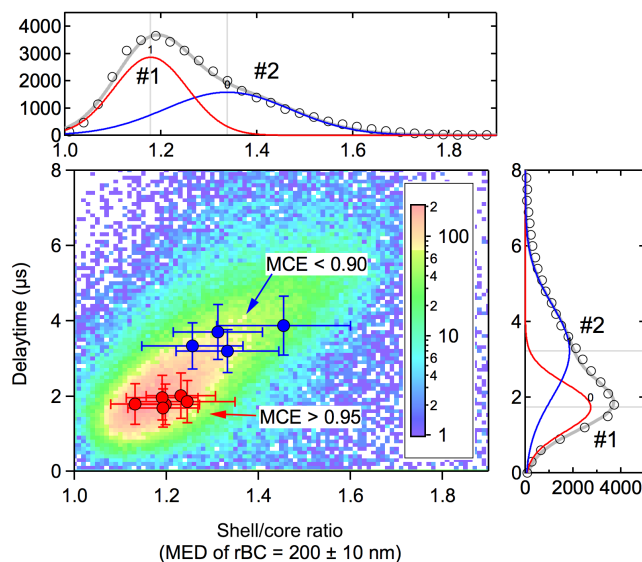

Figure 4. The dependence of the delay time of the peak of incandescence signal *after* that of the scattering signal as a function of the shell/core ratio for the rBC particles with MED $= 200 \pm 10$ nm for all the burning cases, and the multiple Gaussian fitting for all the data of cross sections along the *x*-axis and *y*-axis. For comparison with the curve fitting results, observational data of the flaming-dominant (MCE > 0.95, red circle) and smoldering-dominant (MCE < 0.9, blue circle) cases are also shown in the figure.

ratio between mode no. 1 and mode no. 2 was 0.76. This result suggested that the thinly and thickly coated rBC particles were almost the same. It was worth noting that the histogram of the delay times of rBC-containing particles also had two modes, with one mode occurring at $\Delta t = 1.74$ μs and another peak occurring at $\Delta t = 3.18$ μs. The integrated area ratio between these two modes was 0.78, almost the same as the ratio derived from the S/C mode. This result demonstrates that the rBC-containing particles with rBC cores of 200 nm and S/C ratios of 1.18 and 1.34 corresponded to delay times of 1.74 and 3.18 μs, respectively, at least in this study. Moteki et al. (2007) investigated the relationship between delay time and coating thickness for ambient rBC particles with MED $= 200$ nm, and they reported that the delay time increased linearly from 0–1 to ~ 4 μs as the coating thickness increased up to 200 nm (S/C ratio $= 2$), consistent with our study. It should be noted that the delay time for uncoated rBC particles ($S/C = 1$) was not necessarily zero because of intrinsic differences among SP2 instrumentations. For instance, a shift of $\Delta t^* = 0$–0.6 μs was found for uncoated rBC particles among studies (Moteki et al., 2007; Sedlacek et al., 2012). By subtracting the Δt^* value (0.8 μs) in this study, the Δt was found to be 0.9–2.4 μs for coated rBC particles in the biomass burning plumes.

3.5 Coating thickness of rBC as a function of MCE

Figure 5a depicts the variations in modal Δt values for rBC particles with MED = 200 nm as a function of the MCE value. As shown, Δt clearly decreased as the MCE value increased ($r^2 = 0.63$); the decreasing trend was statistically significant at a level of 5 %. S/C ratios of rBC particles (Fig. 5b) were found to be 1.4 at MCE < 0.9 (smoldering combustion) and 1.2 at MCE > 0.95 (flaming combustion). Such a tendency was mostly due to formation of organic matter at different combustion phases. Collier et al. (2016) reported that organic aerosol emissions had negative correlations with MCE, implying that coating processes of semi-volatile organics played a key role in the increase in the S/C ratio. Variations in both the Δt values and the S/C ratios as a function of MCE showed similar tendencies for particles with MED of the rBC cores ranging between 190 and 250 nm. Airborne measurements during the ARCTAS campaign (Kondo et al., 2011) showed an increasing tendency for the values of the S/C ratio (1.3–1.66) with an increase in MCE, and the authors explained that this phenomenon was because flaming phase plumes were more aged than the smoldering plumes; a 205 ± 40 % increase in the volume of the coating materials resulted in a larger S/C ratio than that of rBC particles in smoldering plumes.

Statistically, the modal coating thickness of rBC particles was found to be ~ 20 nm (Fig. S5). In fact, discrepancies exist among studies due to differences in biomass types, burning conditions and sampling locations. For example, ambient measurements in Europe indicated a coating thickness of rBC particles of 15 nm on average, and more than half of the rBC particles had a coating thinner than 10 nm (Laborde et al., 2013). Airborne measurements reported a thicker coating (65 ± 12 nm) for rBC particles from brush fires (Schwarz et al., 2008).

Table 3 summarizes recent studies that report the coating thicknesses and S/C ratios of rBC particles. Among the studies, the coating thicknesses of freshly emitted rBC particles from burning of wheat residues were smallest, with a mean value of ~ 20 nm. Coating thicknesses of rBC particles from brush fire (Schwarz et al., 2008) and boreal forest (Taylor et al., 2014) were 65 ± 12 and 50–100 nm, respectively. We noticed that there was a large difference in the age of OBB plumes, and coating thicknesses of rBC seemed to increase as they experienced a longer transport period. It implied that aging of particles also played an important role in determining the coating thickness of rBC particles. Further observational investigation on the evolution of OBB process is also needed to explicate the contribution to the total variability. The coating thickness of rBC particles from traffic emissions varied significantly, depending on the urban emission and photochemical processes. The transport pattern and meteorological parameters (such as RH) also play a role in changing the morphology of rBC-containing particles. Fan et al. (2016) reported that the hygroscopic shrinkage effect
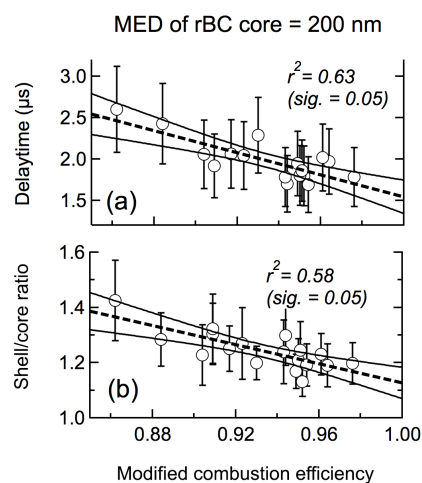

MED of rBC core = 200 nm

Figure 5. Variations in the delay time **(a)** and the shell / core ratio **(b)** as a function of MCE values for rBC particles with MED = 200 ± 10 nm.

under high RH conditions led aggregated soot particles to become more tightly clustered, which resulted in an increase in the shell / core ratios. Such phenomena have also been observed under ambient conditions (Adachi et al., 2010). It has also been reported that condensation and coagulation processes cause the voids of rBC aggregates to be filled or cause the particles to collapse into a compact shell–core structure (Zhang et al., 2008).

3.6 Relationship between the S/C ratio and NMVOCs

Scatter plots of the S/C ratios of rBC particles with core MED = 200 nm plotted against the emission factor (EF, in unit $g\,kg^{-1}$) of each condensable NMVOC are shown in Fig. 6. It is obvious that the S/C ratio increases with the EF for the burning of both dry wheat straw and dry rapeseed plants. As discussed in a previous study (Inomata et al., 2015), the high EF values of the NMVOCs are related to smoldering combustion, in which the production of rBC particles is less effective due to the low-temperature conditions. The condensation of semi-volatile organics was evident under rBC nucleus-limited conditions, resulting in higher S/C ratios. We also found that the S/C ratio from the laboratory burning of rapeseed plants was apparently higher than that of wheat straw under the same NMVOC emissions conditions. This difference is likely attributable to the physical formation processes of rBC particles under high-temperature conditions for different combustion types. For instance, intensive fires tend to produce non-spherical rBC particles with chain-like structures, which display uneven coatings of semi-volatile organics on the rBC particles; however, for compact, quasi-spherical rBC particles, it is much easier to form evenly distributed, thicker coatings. For wheat residues, the S/C ratios (~ 1.4) of rBC for wet samples were apparently higher than those (12–1.3) of dry samples at the same EF.

Table 3. Brief summary of the coating thickness and shell/core (S/C) ratios for rBC emissions from different sources collected from recent studies.

rBC source		Coating thickness	S/C ratio	rBC core size	Age	Sampling description	Study
Biomass burning	Brush fires	65 ± 12 nm	–	[a]190–210 nm	0.5–1.5 h	Airborne SP2 measurements during 2006 Texas Air Quality Study	Schwarz et al. (2008)
		∼ 15 nm		200 nm	–	Field measurements using SP2 in the agglomeration of Paris as part of the MEGAPOLI European project	Laborde et al. (2013)
	Boreal forest	50–100 nm	2.0–2.5	152–196 nm	1–2 days	Airborne SP2 measurement during the second phase of the BORTAS project over eastern Canada and the North Atlantic during July–August 2011.	Taylor et al. (2014)
	Agriculture	–	1.3–1.6	[b]120–140 nm	1–2 h	Airborne SP2 measurements during ARCTAS in spring and summer	Kondo et al. (2011)
	Wheat, rapeseed plant	20 nm (11–54 nm)	1.2–1.4	200 ± 10 nm	< 10 s	Burning experiments in combustion chamber in laboratory environment	This study
Asia continental		–	1.6	200 nm	2–3 days	Ground-based SP2 measurements at	Shiraiwa et
Free troposphere		–	1.3–1.4	200 nm	12 h	Fukue, Japan	al. (2008)
Aged air mass		44 nm	–	200 nm		Field measurement using SP2 in the agglomeration of Paris as part of	Laborde et al. (2013)
Traffic influence		2 ± 10 nm		200 nm		the MEGAPOLI European project	
Traffic emission		110–300 nm		80–130	Highly aged	Ground-based SP2 measurement at an urban site in Shanghai, China	Gong et al. (2016)
Traffic emission		–	1.6–2.4	–	–	Clean Air for London (ClearfLo)	Liu et
Solid fuel burning		–	< 1.2	–	–	experimental campaign in winter, 2012	al. (2014)
Europe continental		–	1.45–1.6	–	–		
Urban emission		20–30 nm		> 200 nm	1–2 days	Airborne SP2 measurement during the MILAGRO campaign	Subramanian et al. (2010)

[a] Volume equivalent diameter; [b] count median diameter.

This result indicates that the microphysical properties of the rBC particles varied under different biomass burning conditions. To answer these questions, further analysis of individual particles using electro-microscopy is needed.

4 Conclusions

In the present study, biomass burning experiments were conducted in the laboratory using wheat straw and rapeseed plants, two major agriculture crop residues, which were obtained from the Yangtze River Delta region (YRDR) during the Rudong field campaign. The combustion state of each biomass burning experiment was assessed using the modified combustion efficiency (MCE) that was calculated on the basis of fire-integrated excess CO and CO_2 mixing ratios, relative to their background values. A full calibration of the single particle soot photometer (SP2) was performed using commercial calibrating particles (fullerene spheres and polystyrene latex particles) following the standard procedures that were proposed by Moteki and Kondo (2007). The mass equivalent diameter (MED) values of the rBC parti-

cles were calculated on the basis of the measured incandescence signals and a presumed rBC density of $1.8\,\mathrm{g\,cm^{-3}}$. The major findings are as follows. (1) The emission ratio of rBC, defined as ΔrBC / ΔCO, increased from 0.2 to $40\,\mathrm{\mu g\,m^{-3}\,ppbv^{-1}}$ as MCE increased from 0.84 to 0.98. The increasing trend was in accordance with previous laboratory studies, and this result was largely insensitive to the type of biomass considered. (2) The mass mode diameter of the rBC particles ranged from 152 to 215 nm. It was found that the rBC particles produced during flaming combustion had larger MMD values than those produced during smoldering combustion. This result indicated that the rBC coagulation/growth process was intensive during flaming combustion as a result of substantial production of rBC precursor particles, such as PAHs, under the high-temperature and oxygen-deprived conditions that occurred within intense flames. (3) For rBC-containing particles, the delay time of the occurrence of the incandescent peak *after* the scattering peak clearly increased as the S/C ratio increased, and smoldering combustion tends to produce more thickly coated rBC particles than flaming combustion. (4) The condensation
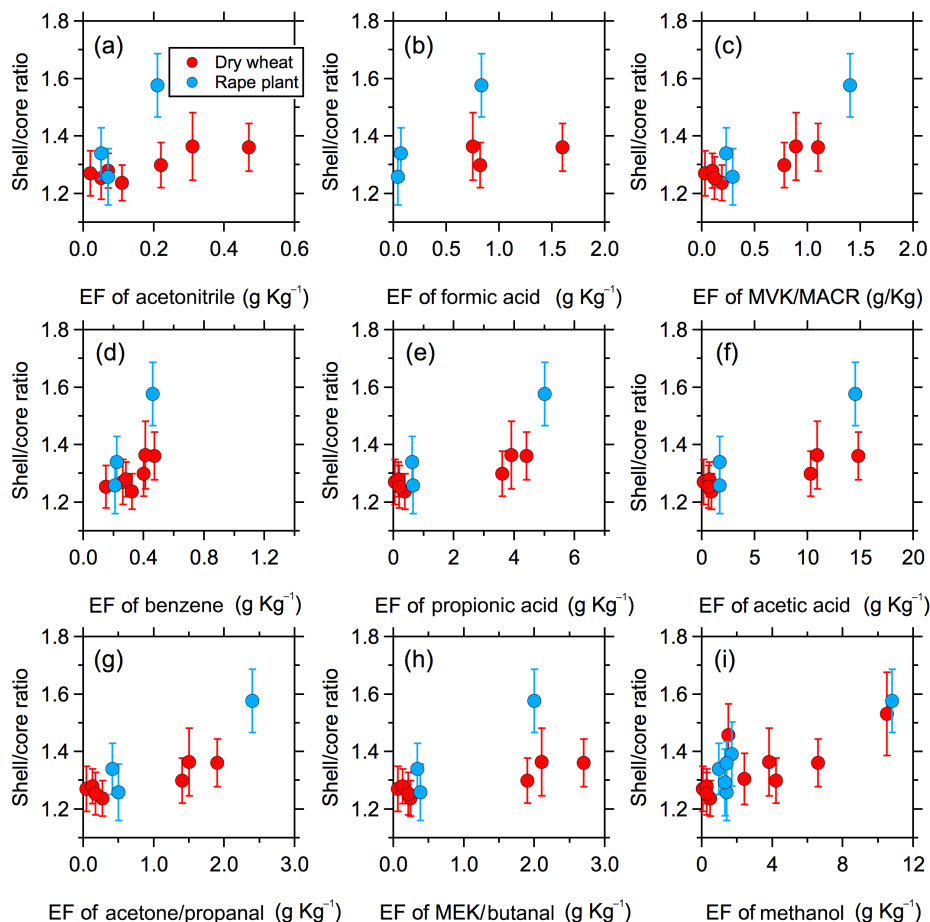
Figure 6. Variations in the shell/core ratios of rBC particles with MED = 200 ± 10 nm as a function of the emission factor of each experiment. Here, EF is defined as the amount of each compound released per unit amount of dry fuel consumed. The red, green and blue colors indicate the dry wheat straw, wet wheat straw and rapeseed plant samples, respectively.

of semi-volatile organics co-emitted by the thermal pyrolysis of biomass plays a key role in the formation of coatings on the surface of rBC particles, though the mixing/coating processes of condensable NMVOCs may vary significantly, probably due to the distinct physical characteristics of rBC particles produced by the burning of wheat straw and rapeseed plants.

Data availability. To request SP2 data for scientific research purposes, please contact Xiaole Pan at the Institute of Atmospheric Physics, Chinese Academy of Sciences, via email (panxiaole@mail.iap.ac.cn).

The Supplement related to this article is available online at https://doi.org/10.5194/acp-17-13001-2017-supplement.

References

Adachi, K., Chung, S. H., and Buseck, P. R.: Shapes of soot aerosol particles and implications for their effects on climate, J. Geophys. Res.-Atmos., 115, D15206, https://doi.org/10.1029/2009JD012868, 2010.

Akagi, S. K., Yokelson, R. J., Wiedinmyer, C., Alvarado, M. J., Reid, J. S., Karl, T., Crounse, J. D., and Wennberg, P. O.: Emission factors for open and domestic biomass burning for use

in atmospheric models, Atmos. Chem. Phys., 11, 4039–4072, https://doi.org/10.5194/acp-11-4039-2011, 2011.

Andreae, M. O. and Merlet, P.: Emission of trace gases and aerosols from biomass burning, Global Biogeochem. Cy., 15, 955–966, 2001.

Bond, T. C., Streets, D. G., Yarber, K. F., Nelson, S. M., Woo, J.-H., and Klimont, Z.: A technology-based global inventory of black and organic carbon emissions from combustion, J. Geophys. Res., 109, D14203, https://doi.org/10.1029/2003JD003697, 2004.

Bond, T. C., Doherty, S. J., Fahey, D. W., Forster, P. M., Berntsen, T., DeAngelo, B. J., Flanner, M. G., Ghan, S., Kärcher, B., and Koch, D.: Bounding the role of black carbon in the climate system: A scientific assessment, J. Geophys. Res.-Atmos., 118, 5380–5552, 2013.

Cappa, C. D., Onasch, T. B., Massoli, P., Worsnop, D. R., Bates, T. S., Cross, E. S., Davidovits, P., Hakala, J., Hayden, K. L., and Jobson, B. T.: Radiative absorption enhancements due to the mixing state of atmospheric black carbon, Science, 337, 1078–1081, 2012.

Chen, L.-W. A., Verburg, P., Shackelford, A., Zhu, D., Susfalk, R., Chow, J. C., and Watson, J. G.: Moisture effects on carbon and nitrogen emission from burning of wildland biomass, Atmos. Chem. Phys., 10, 6617–6625, https://doi.org/10.5194/acp-10-6617-2010, 2010.

Collier, S., Zhou, S., Onasch, T. B., Jaffe, D. A., Kleinman, L., Sedlacek, A. J., Briggs, N. L., Hee, J., Fortner, E., Shilling, J. E., Worsnop, D., Yokelson, R. J., Parworth, C., Ge, X., Xu, J., Butterfield, Z., Chand, D., Dubey, M. K., Pekour, M. S., Springston, S., and Zhang, Q.: Regional Influence of Aerosol Emissions from Wildfires Driven by Combustion Efficiency: Insights from the BBOP Campaign, Environ. Sci. Technol., 50, 8613–8622, https://doi.org/10.1021/acs.est.6b01617, 2016.

Fan, M., Chen, L., Li, S., Zou, M., Su, L., and Tao, J.: The effects of morphology and water coating on the optical properties of soot aggregates, Aerosol Air Qual. Res., 16, 1315–1326, 2016.

Gao, R., Schwarz, J., Kelly, K., Fahey, D., Watts, L., Thompson, T., Spackman, J., Slowik, J., Cross, E., and Han, J.-H.: A novel method for estimating light-scattering properties of soot aerosols using a modified single-particle soot photometer, Aerosol Sci. Tech., 41, 125–135, 2007.

Gilardoni, S., Massoli, P., Paglione, M., Giulianelli, L., Carbone, C., Rinaldi, M., Decesari, S., Sandrini, S., Costabile, F., and Gobbi, G. P.: Direct observation of aqueous secondary organic aerosol from biomass-burning emissions, P. Natl. Acad. Sci. USA, 113, 10013–10018, 2016.

Gong, X., Zhang, C., Chen, H., Nizkorodov, S. A., Chen, J., and Yang, X.: Size distribution and mixing state of black carbon particles during a heavy air pollution episode in Shanghai, Atmos. Chem. Phys., 16, 5399–5411, https://doi.org/10.5194/acp-16-5399-2016, 2016.

Gysel, M., Laborde, M., Olfert, J. S., Subramanian, R., and Gröhn, A. J.: Effective density of Aquadag and fullerene soot black carbon reference materials used for SP2 calibration, Atmos. Meas. Tech., 4, 2851–2858, https://doi.org/10.5194/amt-4-2851-2011, 2011.

He, C., Liou, K.-N., Takano, Y., Zhang, R., Levy Zamora, M., Yang, P., Li, Q., and Leung, L. R.: Variation of the radiative properties during black carbon aging: theoretical and experi-

mental intercomparison, Atmos. Chem. Phys., 15, 11967–11980, https://doi.org/10.5194/acp-15-11967-2015, 2015.

Healy, R. M., Wang, J. M., Jeong, C. H., Lee, A. K. Y., Willis, M. D., Jaroudi, E., Zimmerman, N., Hilker, N., Murphy, M., and Eckhardt, S.: Light-absorbing properties of ambient black carbon and brown carbon from fossil fuel and biomass burning sources, J. Geophys. Res.-Atmos., 120, 6619–6633, 2015.

Inomata, S., Tanimoto, H., Pan, X., Taketani, F., Komazaki, Y., Miyakawa, T., Kanaya, Y., and Wang, Z.: Laboratory measurements of emission factors of nonmethane volatile organic compounds from burning of Chinese crop residues, J. Geophys. Res.-Atmos., 120, 5237–5252, 2015.

Jacobson, M. Z.: Strong radiative heating due to the mixing state of black carbon in atmospheric aerosols, Nature, 409, 695–697, 2001.

Kondo, Y., Matsui, H., Moteki, N., Sahu, L., Takegawa, N., Kajino, M., Zhao, Y., Cubison, M. J., Jimenez, J. L., Vay, S., Diskin, G. S., Anderson, B., Wisthaler, A., Mikoviny, T., Fuelberg, H. E., Blake, D. R., Huey, G., Weinheimer, A. J., Knapp, D. J., and Brune, W. H.: Emissions of black carbon, organic, and inorganic aerosols from biomass burning in North America and Asia in 2008, J. Geophys. Res., 116, D08204, https://doi.org/10.1029/2010jd015152, 2011.

Kudo, S., Tanimoto, H., Inomata, S., Saito, S., Pan, X., Kanaya, Y., Taketani, F., Wang, Z., Chen, H., and Dong, H.: Emissions of nonmethane volatile organic compounds from open crop residue burning in the Yangtze River Delta region, China, J. Geophys. Res.-Atmos., 119, 7684–7698, 2014.

Laborde, M., Mertes, P., Zieger, P., Dommen, J., Baltensperger, U., and Gysel, M.: Sensitivity of the Single Particle Soot Photometer to different black carbon types, Atmos. Meas. Tech., 5, 1031–1043, https://doi.org/10.5194/amt-5-1031-2012, 2012.

Laborde, M., Crippa, M., Tritscher, T., Jurányi, Z., Decarlo, P. F., Temime-Roussel, B., Marchand, N., Eckhardt, S., Stohl, A., Baltensperger, U., Prévôt, A. S. H., Weingartner, E., and Gysel, M.: Black carbon physical properties and mixing state in the European megacity Paris, Atmos. Chem. Phys., 13, 5831–5856, https://doi.org/10.5194/acp-13-5831-2013, 2013.

Lack, D. A., Langridge, J. M., Bahreini, R., Cappa, C. D., Middlebrook, A. M., and Schwarz, J. P.: Brown carbon and internal mixing in biomass burning particles, P. Natl. Acad. Sci. USA, 109, 14802–14807, 2012.

Lack, D. A., Moosmüller, H., McMeeking, G. R., Chakrabarty, R. K., and Baumgardner, D.: Characterizing elemental, equivalent black, and refractory black carbon aerosol particles: a review of techniques, their limitations and uncertainties, Anal. Bioanal. Chem., 406, 99–122, 2014.

Lee, K. W. and Chen, H.: Coagulation rate of polydisperse particles, Aerosol Sci. Tech., 3, 327–334, 1984.

Liu, D., Allan, J. D., Young, D. E., Coe, H., Beddows, D., Fleming, Z. L., Flynn, M. J., Gallagher, M. W., Harrison, R. M., Lee, J., Prevot, A. S. H., Taylor, J. W., Yin, J., Williams, P. I., and Zotter, P.: Size distribution, mixing state and source apportionment of black carbon aerosol in London during wintertime, Atmos. Chem. Phys., 14, 10061–10084, https://doi.org/10.5194/acp-14-10061-2014, 2014.

Liu, D., Taylor, J. W., Young, D. E., Flynn, M. J., Coe, H., and Allan, J. D.: The effect of complex black carbon microphysics on the determination of the optical properties of brown carbon, Geophys.

Res. Lett., 42, 613–619, https://doi.org/10.1002/2014GL062443, 2015.

Liu, S., Aiken, A. C., Gorkowski, K., Dubey, M. K., Cappa, C. D., Williams, L. R., Herndon, S. C., Massoli, P., Fortner, E. C., and Chhabra, P. S.: Enhanced light absorption by mixed source black and brown carbon particles in UK winter, Nat. Commun., 6, 8435, https://doi.org/10.1038/ncomms9435, 2015.

Massoli, P., Onasch, T. B., Cappa, C. D., Nuamaan, I., Hakala, J., Hayden, K., Li, S. M., Sueper, D. T., Bates, T. S., and Quinn, P. K.: Characterization of black carbon-containing particles from soot particle aerosol mass spectrometer measurements on the R/V *Atlantis* during CalNex 2010, J. Geophys. Res.-Atmos., 120, 2575–2593, 2015.

May, A. A., McMeeking, G. R., Lee, T., Taylor, J. W., Craven, J. S., Burling, I., Sullivan, A. P., Akagi, S., Collett, J. L., and Flynn, M.: Aerosol emissions from prescribed fires in the United States: A synthesis of laboratory and aircraft measurements, J. Geophys. Res.-Atmos., 119, 11826–11849, https://doi.org/10.1002/2014JD021848, 2014.

Mazzoleni, L. R., Zielinska, B., and Moosmüller, H.: Emissions of levoglucosan, methoxy phenols, and organic acids from prescribed burns, laboratory combustion of wildland fuels, and residential wood combustion, Environ. Sci. Technol., 41, 2115–2122, 2007.

McMeeking, G. R., Kreidenweis, S. M., Baker, S., Carrico, C. M., Chow, J. C., Collett, J. L., Hao, W. M., Holden, A. S., Kirchstetter, T. W., and Malm, W. C.: Emissions of trace gases and aerosols during the open combustion of biomass in the laboratory, J. Geophys. Res.-Atmos., 114, D19210, https://doi.org/10.1029/2009JD011836, 2009.

Miyakawa, T., Kanaya, Y., Komazaki, Y., Taketani, F., Pan, X., Irwin, M., and Symonds, J.: Intercomparison between a single particle soot photometer and evolved gas analysis in an industrial area in Japan: Implications for the consistency of soot aerosol mass concentration measurements, Atmos. Environ., 127, 14–21, https://doi.org/10.1016/j.atmosenv.2015.12.018, 2016.

Moteki, N. and Kondo, Y.: Effects of Mixing State on Black Carbon Measurements by Laser-Induced Incandescence, Aerosol Sci. Tech., 41, 398–417, 2007.

Moteki, N. and Kondo, Y.: Dependence of laser-induced incandescence on physical properties of black carbon aerosols: Measurements and theoretical interpretation, Aerosol Sci. Tech., 44, 663–675, 2010.

Moteki, N., Kondo, Y., Miyazaki, Y., Takegawa, N., Komazaki, Y., Kurata, G., Shirai, T., Blake, D. R., Miyakawa, T., and Koike, M.: Evolution of mixing state of black carbon particles: Aircraft measurements over the western Pacific in March 2004, Geophys. Res. Lett., 34, L11803, https://doi.org/10.1029/2006GL028943, 2007.

Moteki, N., Kondo, Y., and Adachi, K.: Identification by single-particle soot photometer of black carbon particles attached to other particles: Laboratory experiments and ground observations in Tokyo, J. Geophys. Res.-Atmos., 119, 1031–1043, 2014.

Novakov, T., Menon, S., Kirchstetter, T. W., Koch, D., and Hansen, J. E.: Aerosol organic carbon to black carbon ratios: Analysis of published data and implications for climate forcing, J. Geophys. Res., 110, D21205, https://doi.org/10.1029/2005jd005977, 2005.

Pan, X. L., Kanaya, Y., Wang, Z. F., Liu, Y., Pochanart, P., Akimoto, H., Sun, Y. L., Dong, H. B., Li, J., Irie, H., and Takigawa, M.: Correlation of black carbon aerosol and carbon monoxide in the high-altitude environment of Mt. Huang in Eastern China, Atmos. Chem. Phys., 11, 9735–9747, https://doi.org/10.5194/acp-11-9735-2011, 2011.

Pan, X. L., Kanaya, Y., Wang, Z., Taketani, F., Tanimoto, H., Irie, H., Takashima, H., and Inomata, S.: Emission ratio of carbonaceous aerosols observed near crop residual burning sources in a rural area of the Yangtze River Delta Region, China, J. Geophys. Res.-Atmos., 117, D22304, https://doi.org/10.1029/2012JD018357, 2012.

Pan, X. L., Kanaya, Y., Wang, Z. F., Komazaki, Y., Taketani, F., Akimoto, H., and Pochanart, P.: Variations of carbonaceous aerosols from open crop residue burning with transport and its implication to estimate their lifetimes, Atmos. Environ., 74, 301–310, 2013.

Pósfai, M., Gelencsér, A., Simonics, R., Arató, K., Li, J., Hobbs, P. V., and Buseck, P. R.: Atmospheric tar balls: Particles from biomass and biofuel burning, J. Geophys. Res.-Atmos., 109, D06213, https://doi.org/10.1029/2003JD004169, 2004.

Ramanathan, V. and Carmichael, G.: Global and regional climate changes due to black carbon, Nat. Geosci., 1, 221–227, 2008.

Reid, J. S., Koppmann, R., Eck, T. F., and Eleuterio, D. P.: A review of biomass burning emissions part II: intensive physical properties of biomass burning particles, Atmos. Chem. Phys., 5, 799–825, https://doi.org/10.5194/acp-5-799-2005, 2005.

Saleh, R., Robinson, E. S., Tkacik, D. S., Ahern, A. T., Liu, S., Aiken, A. C., Sullivan, R. C., Presto, A. A., Dubey, M. K., and Yokelson, R. J.: Brownness of organics in aerosols from biomass burning linked to their black carbon content, Nat. Geosci., 7, 647–650, https://doi.org/10.1038/ngeo2220, 2014.

Saleh, R., Marks, M., Heo, J., Adams, P. J., Donahue, N. M., and Robinson, A. L.: Contribution of brown carbon and lensing to the direct radiative effect of carbonaceous aerosols from biomass and biofuel burning emissions, J. Geophys. Res.-Atmos., 120, 10285–10296, https://doi.org/10.1002/2015JD023697, 2015.

Schwarz, J. P., Gao, R. S., Spackman, J. R., Watts, L. A., Thomson, D. S., Fahey, D. W., Ryerson, T. B., Peischl, J., Holloway, J. S., and Trainer, M.: Measurement of the mixing state, mass, and optical size of individual black carbon particles in urban and biomass burning emissions, Geophys. Res. Lett., 35, L13810, https://doi.org/10.1029/2008GL033968, 2008.

Schwarz, J. P., Spackman, J., Gao, R., Perring, A., Cross, E., Onasch, T., Ahern, A., Wrobel, W., Davidovits, P., and Olfert, J.: The detection efficiency of the single particle soot photometer, Aerosol Sci. Tech., 44, 612–628, https://doi.org/10.1080/02786826.2010.481298, 2010.

Sedlacek, A. J., Lewis, E. R., Kleinman, L., Xu, J., and Zhang, Q.: Determination of and evidence for non-core-shell structure of particles containing black carbon using the Single-Particle Soot Photometer (SP2), Geophys. Res. Lett., 39, L06802, https://doi.org/10.1029/2012GL050905, 2012.

Sedlacek, A. J., Lewis, E. R., Onasch, T. B., Lambe, A. T., and Davidovits, P.: Investigation of refractory black carbon-containing particle morphologies using the single-particle soot photometer (SP2), Aerosol Sci. Tech., 49, 872–885, 2015.

Shiraiwa, M., Kondo, Y., Moteki, N., Takegawa, N., Sahu, L. K., Takami, A., Hatakeyama, S., Yonemura, S., and Blake, D. R.: Radiative impact of mixing state of black carbon aerosol in Asian outflow, J. Geophys. Res.-Atmos., 113, D24210, https://doi.org/10.1029/2008JD010546, 2008.

Shiraiwa, M., Kondo, Y., Iwamoto, T., and Kita, K.: Amplification of light absorption of black carbon by organic coating, Aerosol Sci. Tech., 44, 46–54, 2010.

Spackman, J. R., Schwarz, J. P., Gao, R. S., Watts, L. A., Thomson, D. S., Fahey, D. W., Holloway, J. S., de Gouw, J. A., Trainer, M., and Ryerson, T. B.: Empirical correlations between black carbon aerosol and carbon monoxide in the lower and middle troposphere, Geophys. Res. Lett., 35, L19816, https://doi.org/10.1029/2008gl035237, 2008.

Subramanian, R., Kok, G. L., Baumgardner, D., Clarke, A., Shinozuka, Y., Campos, T. L., Heizer, C. G., Stephens, B. B., de Foy, B., Voss, P. B., and Zaveri, R. A.: Black carbon over Mexico: the effect of atmospheric transport on mixing state, mass absorption cross-section, and BC / CO ratios, Atmos. Chem. Phys., 10, 219–237, https://doi.org/10.5194/acp-10-219-2010, 2010.

Taylor, J. W., Allan, J. D., Allen, G., Coe, H., Williams, P. I., Flynn, M. J., Le Breton, M., Muller, J. B. A., Percival, C. J., Oram, D., Forster, G., Lee, J. D., Rickard, A. R., Parrington, M., and Palmer, P. I.: Size-dependent wet removal of black carbon in Canadian biomass burning plumes, Atmos. Chem. Phys., 14, 13755–13771, https://doi.org/10.5194/acp-14-13755-2014, 2014.

Ueda, S., Nakayama, T., Taketani, F., Adachi, K., Matsuki, A., Iwamoto, Y., Sadanaga, Y., and Matsumi, Y.: Light absorption and morphological properties of soot-containing aerosols observed at an East Asian outflow site, Noto Peninsula, Japan, Atmos. Chem. Phys., 16, 2525–2541, https://doi.org/10.5194/acp-16-2525-2016, 2016.

Warneke, C., Bahreini, R., Brioude, J., Brock, C. A., De Gouw, J. A., Fahey, D. W., Froyd, K. D., Holloway, J. S., Middlebrook, A., and Miller, L.: Biomass burning in Siberia and Kazakhstan as an important source for haze over the Alaskan Arctic in April 2008, Geophys. Res. Lett., 36, L02813, https://doi.org/10.1029/2008GL036194, 2009.

Yan, X., Ohara, T., and Akimoto, H.: Bottom-up estimate of biomass burning in mainland China, Atmos. Environ., 40, 5262–5273, 2006.

Yokelson, R. J., Susott, R., Ward, D. E., Reardon, J., and Griffith, D. W. T.: Emissions from smoldering combustion of biomass measured by open-path Fourier transform infrared spectroscopy, J. Geophys. Res.-Atmos., 102, 18865–18877, 1997.

Zhang, R., Khalizov, A. F., Pagels, J., Zhang, D., Xue, H., and McMurry, P. H.: Variability in morphology, hygroscopicity, and optical properties of soot aerosols during atmospheric processing, P. Natl. Acad. Sci. USA, 105, 10291–10296, https://doi.org/10.1073/pnas.0804860105, 2008.